THE ASTROPHYSICAL JOURNAL, 303:659–666, 1986 April 15

ROTATION MEASURES OF EXTRAGALACTIC RADIO SOURCES VIEWED THROUGH THE MOLECULAR CLOUDS CEPHEUS A AND L1551

J. H. SIMONETTI[1] AND J. M. CORDES[2]
Department of Astronomy, Cornell University, and the National Astronomy and Ionosphere Center
Received 1985 August 16; accepted 1985 October 15

ABSTRACT

Faraday rotation measures of background extragalactic radio sources behind high-velocity molecular flows were determined to help constrain magnetic fields in and near the molecular flows.

Rotation measures of seven sources within a $\sim 20'$ wide area seen through Cep A fall in two groups separated by ~ 150 rad m^{-2}—which is a large difference, given previous knowledge of rotation measure variations on small angular scales. It is not clear whether the variation of rotation measure is determined by the high-velocity material or by larger scale structure in the Cep A region.

For L1551, we obtained $\Delta \mathrm{RM} \approx 30$ rad m^{-2} between a line of sight directly through the NE lobe of the high-velocity CO and another $7'$ away. A wide range of magnetic field strength associated with the molecular flow is possible. A hard lower limit of 2 μG requires the presence of a region of high ionization ($n_e \approx 10^2$ cm^{-3}) of path length comparable to the thickness of the molecular flow region (~ 0.1 pc). Larger, 10–100 μG field values are more likely. Several bipolar flow models are discussed with an emphasis on the availability of free electrons. It appears substantial shock ionization must take place, requiring relative gas velocities greater than 50 km s^{-1} if excessively large magnetic field strengths and implications inconsistent with the observed flow are to be avoided.

Subject headings: interstellar: magnetic fields — interstellar: molecules — polarization

I. INTRODUCTION

Magnetic fields may influence the morphology and dynamics of the high-velocity molecular flows associated with young stellar objects. In stellar-wind driven flows, where a wind-filled bubble expands into the ambient molecular cloud pushing out a shell of molecular gas, magnetic stresses at the cavity's surface may directly affect evolution. Anisotropy in the ambient cloud's density distribution, perhaps determined by magnetic field structure, may be responsible for the bipolar structure that is often seen (Königl 1982). The formation of disks or toroids around central protostars is perhaps governed by a combination of magnetic fields and rotation. In another model (Pudritz and Norman 1983, 1986; Pudritz 1985), the molecular flow itself and an interior, higher velocity ionized wind are driven centrifugally from a rotating, magnetized molecular disk. In an interstellar-bullet model (Chevalier 1980; Norman and Silk 1979), knot dynamics may depend upon ambient fields, while a collimating disk would be affected by magnetic fields as in the wind models. Draine (1983) has proposed a model for a magnetic-pressure–driven flow where the magnetic field of the collapsing protostar transfers energy from the protostar to the surrounding medium.

Our present understanding of the molecular emission lines, presumably from shocks in the high-velocity flow region, is dependent upon models of magnetohydrodynamic shocks in the molecular gas. Preshock magnetic fields of milligauss strength have thus been inferred for the Orion flow (Draine and Roberge 1982; Chernoff, Hollenbach, and McKee 1982). Theoretical modeling of cloud collapse also implies typical fields of this strength (Mouschovias 1976).

Observationally, the uniformity of starlight polarization vectors across the dark cloud L1551 (Vrba, Strom, and Strom 1976) supports Königl's conception of a flow region where the ambient magnetic field is an important factor in the cloud structure. Observations of Zeeman splitting in an OH maser in the Cep A flow area (Wouterloot, Habing, and Herman 1980) yield a magnetic field of 3.5 mG, but this value must apply only to the large-density region near the maser. Hughes and Wouterloot (1984) infer a roughly uniform ~ 1 mG field through Cep A from observations of a linear arrangement of elongated H II regions at the center of the Cep A condensation and the assumption that a magnetic field is responsible for confinement (i.e., $B^2/8\pi > nkT$). However, the direction of their field is perpendicular to that which would be consistent with Königl's (1982) model as applied to the Cep A flow. Certainly, measurements of the magnetic field strength in and about molecular flows would be valuable for determining whether the field is dynamically important.

To constrain the magnetic field within a localized region (e.g., a molecular flow) we compare Faraday rotation measures (RMs) for lines of sight toward two or more extragalactic objects: one through the region of interest, the other close to but excluding the region. The rotation measure is given by

$$\mathrm{RM} = 0.81 \int_0^L dl\, n_e B_{\|} \text{ rad m}^{-2} , \qquad (1)$$

for path length L (pc), electron density n_e (cm^{-3}), and magnetic field component parallel to the line of sight $B_{\|}$ (microgauss), and is obtained from observations taken at different wavelengths λ as

$$\mathrm{RM} = d\psi/d(\lambda^2) , \qquad (2)$$

where ψ is the position angle of linearly polarized radiation. If we can demonstrate that the only important difference in the

[1] The National Radio Astronomy Observatory, which is operated by Associated Universities, Inc., under contract with the National Science Foundation.

[2] Alfred P. Sloan Foundation Fellow.

lines of sight is the object under study, then a significant RM difference implies a localized enhancement (or absence) of the product of $n_e B_{\|}$.

In order to use differential Faraday rotation to constrain the product $n_e B_{\|}$ in a localized region, we must demonstrate that the contribution from widespread galactic plasma is small and that intrinsic rotation measures in radio sources are also small. In another study (Simonetti, Cordes, and Spangler 1984; Simonetti and Cordes 1986) we have shown that the RM differences between arbitrarily chosen lines of sight are usually small ($|\Delta \mathrm{RM}| \lesssim 10$ rad m^{-2}) for angular separations $\delta\theta \lesssim 1°$. Optically thin synchrotron sources with high degrees of linear polarization, or little decrease in polarization percentage with increasing λ, have small internal Faraday depths. Most extragalactic sources are believed to have internal rotation measures $\lesssim 10$ rad m^{-2}, since larger values occur only for lines of sight near the galactic plane or through special regions near the solar neighborhood of the Galaxy, except in rare instances. Therefore, it appears quite feasible to use differential RM measurements to measure enhancements in $n_e B_{\|}$ due to particular galactic regions.

We have determined rotation measures of extragalactic sources behind and offset from the high-velocity molecular flows in Cep A and L1551. The results for Cep A are difficult to interpret in terms of a localized magnetic field value, but they seem to suggest substantial variations in the magnetic field strength or direction on the scale of the molecular cloud, and are possibly influenced by the high-velocity flow. A field strength perhaps as large as ~ 0.1 mG is implied by our data for the L1551 region.

II. OBSERVING PROCEDURE

a) *Pilot Survey*

In 1983 April we conducted a search for polarized sources within a VLA primary beam (30′ at $\lambda 20$ cm) centered on 11 high-velocity molecular flow regions. Cloud sizes were larger in some cases than the primary beam, but the flow regions ranged in size from a few to ~ 10 arcmin^2. The search was done in the C-configuration at 1465 MHz using a bandwidth of 50 MHz and 25 minute integrations on each field for a theoretical 3 σ sensitivity of 0.24 mJy per beam. We were hoping to find a strong source behind one or more clouds so that an accurate rotation measure could later be obtained through multifrequency observations. Assuming 10% linear polarization, a 5 σ measurement of polarized flux after ~ 4 hr integration at λ-20 cm requires a 1.5 mJy source. There should be approximately one such source in a 14 arcmin^2 area (Bridle 1982; Condon and Mitchell 1982). The search yielded one field (L1551) where a strong source lies behind the molecular flow and one field (Cep A) where numerous polarized sources in the vicinity of the flow made further observations attractive. For the other fields, sufficiently strong, polarized sources were not found (Table 1).

b) *Cep A and L1551*

Cep A was observed on 1984 February 6, L1551 on 1984 February 13. To isolate source components with little intrinsic Faraday rotation, the B-configuration of the VLA was used. It was necessary to choose both closely and widely spaced observing frequencies to eliminate $n\pi$ position angle ambiguities as well as to make as precise a measurement of RM as possible.

TABLE 1

MOLECULAR FLOW REGIONS WITHOUT POLARIZED EXTRAGALACTIC RADIO SOURCES[a]

Region	R.A. (1950.0)	Decl. (1950.0)
W3 IRS 5	02^{h}21^{m}53^s	61°52′21″
GL 490	03 23 41	58 36 52
T Tauri	04 19 04	19 25 05
Orion A	05 32 47	−05 24 17
NGC 2071	05 44 30	00 20 40
Mon R2	06 05 22	−06 22 25
S255 IRS 1	06 09 59	18 00 15
CRL 961	06 31 59	04 15 09
ρ Oph (BZ 6)	16 23 59	−24 19 49

[a] See text for sensitivity of observations.

Accurate position angle measurements were sought for four frequencies in the 20 cm wavelength L band (1370, 1475, 1590, and 1640 MHz) and one in C band at ~ 4870 MHz. Restricted observing bandwidths (12.5 MHz) at 20 cm minimized Faraday depolarization across these bandpasses, while in C band a 50 MHz bandwidth was used for L1551, and 100 MHz for Cep A. Through sufficiently long integration times, a precision of better than $\pm 10°$ was theoretically obtainable at each source peak for each frequency.

Alternating integrations were carried out on each program source and a nearby calibration point source, with interspersed integrations on 3C 48 to calibrate the flux density scale and on 3C 138 for absolute position angle calibration. For Cep A the phase and amplitude calibration source (2352+495) also served in calibration of the instrumental polarization. Because of the lower declination of L1551, its phase and amplitude calibration source (0428+205) could not be observed at a sufficiently wide range of parallactic angles to enable solution for the instrumental polarization of the array. Therefore, another source (3C 84) was observed at intervals throughout the L1551 session. To limit the effects of beamwidth smearing on sources distant from the observing phase center, two phase centers were chosen for Cep A; L1551 required two phase centers at C band only. Approximately 40 minutes total on-source integration times were accumulated at each frequency for Cep A and L1551.

III. REDUCTION AND ANALYSIS

Polarized intensity, polarization position angle, and cleaned total intensity maps of the primary beam area were produced using the NRAO Astronomical Image Processing System (AIPS). In all cases, maps of $I_{\mathrm{pol}} = (Q^2 + U^2)^{1/2}$ and $\psi = \frac{1}{2} \tan^{-1}(U/Q)$ were made from "dirty" maps of the Stokes parameters Q and U since detectable sidelobe patterns were absent in the "dirty" maps. UV data on Cep A were "tapered" (Gaussian weighted with a 30% level at a 30 kλ baseline) at each frequency to enable full primary beam mapping with a minimum number of pixels, thus reducing processing time. The extragalactic sources in the Cep A field were unresolved without tapering, except for the double source near the field center (see below) whose component separation was large, so no information was lost by reducing resolution. No UV tapering was done at L band for L1551 data; full resolution proved useful in isolating separate components of the sources for the RM analysis. C band data for L1551 were tapered at 20 kλ, resulting in a synthesized beamwidth of approximately equal

TABLE 2

MAP PARAMETERS

Field	Frequency (MHz)	$\sigma_{I_{tot}}$[a]	$\sigma_{I_{pol}}$[a]	Synthesized Beam[b] HPBW	P.A.	Pixel Size
Cep A	1370	0.50	0.11	9.″4 × 9.″4	0°	4″ × 4″
	1475	0.46	0.11	9.4 × 9.4	0	4 × 4
	1590	0.50	0.13	9.4 × 9.4	0	4 × 4
	1640	0.40	0.10	9.4 × 9.4	0	4 × 4
	4860.1	0.13	0.06	4.7 × 4.7	0	2 × 2
L1551	1370	0.19	0.08	4.8 × 4.5	66	1 × 1
	1475	0.15	0.07	4.6 × 4.1	64	1 × 1
	1590	0.13	0.07	4.1 × 3.8	66	1 × 1
	1640	0.12	0.07	4.0 × 3.6	68	1 × 1
	4885.1	0.14	0.10	6.2 × 6.1	30	2 × 2

[a] 1 σ rms variations in map in an area away from any source. In millijanskys per beam.

[b] Major and minor axis half-power widths and position angle of major axis.

size at L and C bands. Tables 2 and 3 display final map and polarized source parameters.

For each source the rotation measure was obtained from a linear least-squares fit of position angle ψ to λ^2, weighting data points by $1/\sigma_\psi^2$ where $\sigma_\psi = \frac{1}{2}\sigma_{I_{pol}}/I_{pol}$ (an accurate position angle uncertainty for $I_{pol} \gg \sigma_{I_{pol}}$; Wardle and Kronberg 1974). Where the polarized intensity at a given frequency is less than 3 times the rms level of the polarized intensity map, the position angle data were ignored. For a reduced χ^2 near unity, the squared uncertainty in RM was estimated by summing the $(\partial \mathrm{RM}/\partial\psi_i)^2\sigma_{\psi_i}^2$, or for large χ^2, computed using the variance of the ψ_i about the fitted line. The position angles are ambiguous by $n\pi$. To compute an accurate RM for a given pixel, these ambiguities were eliminated before the fitting procedure by requiring $|\psi_{1640} - \psi_{1590}|$ to be less than 90° and the position angle at the other frequencies to lie within ±90° of a $\psi(\lambda^2)$ line using ψ_{1640} and ψ_{1590}. Since $|\psi_{1640} - \psi_{1590}| = 180°$ is equivalent to $|\mathrm{RM}| = 1472$ rad m^{-2}, a very large rotation measure, the small $|\psi_{1640} - \psi_{1590}|$ found in practice is probably correct.

Rotation measures were calculated for one pixel at the peak of the unresolved sources in the Cep A field (Figs. 1 and 2). The two polarized sources in the L1551 field were resolved into separate components, each of which were either unresolved or partially resolved. Only one component in the north source N is polarized, while there are two polarized components in the S source. Rotation measures calculated from individual pixels of peak polarized intensity (Figs. 3–6) agreed within the quoted uncertainties with values calculated by averaging over a range of pixels near the peak intensity. The rotation measures of seven sources from the catalog of Simard-Normandin, Kronberg, and Button (1981), which lie within ~10° of L1551, are in the range from approximately −50 to +50 rad m^{-2} and are therefore consistent with our results. There are no sources listed in this catalog within ~10° of Cep A, but our field does lie just inside a region of generally large, negative RMs ($|\mathrm{RM}| \approx 120$ rad m^{-2}) centered just below the plane of the Galaxy.

IV. DISCUSSION

a) *Cep A*

The observed RM values for the sources in the Cep A field are large, and given the fairly tight groupings of values we conclude that any intrinsic contributions from the sources are most likely smaller than the quoted uncertainties. We also expect any errors introduced through the vectorial addition of individual, polarized components in the unresolved sources are less than our stated uncertainties.

As shown in Figure 2, virtually all the lines of sight for which we have RMs pass through the region of CO emission mapped by Sargent (1977), while none pierce the region of high-velocity molecular gas as mapped in CO. However, recent observations of L1551 by Mirabel *et al.* (1984) show high-velocity OH reaching further along the flow axes than high-velocity CO.

TABLE 3

SOURCE PARAMETERS

Field	Source	R.A. (1950.0)	Decl. (1950.0)	Band[a]	I_{tot}^{peak} (mJy/beam)	I_{pol}^{peak} (mJy/beam)	m[b] (%)
Cep A[c]	1	22^{h}55^{m}14^s.5	61°59′05″	L	8	1.6	4.2
	2	22 54 18.0	62 06 25	L	54	4.5	8.3
	3	22 53 28.0	62 01 38	L	23	1.0	4.3
	4	22 52 27.5	61 53 40	L	51	2.1	4.1
	5a	22 53 42.0	61 52 50	L	3.5	0.86	25
				C	1.5	0.27	18
	5b	22 53 32.0	61 53 10	L	3.3	0.82	25
				C	1.0	0.30	30
	6	22 54 56.7	61 42 30	L	6.7	1.1	16
				C	0.7	0.27	39
	7	22 54 48.7	61 41 45	L	14	0.94	6.7
				C	1.2	0.31	26
L1551	N(A)	04 28 49.8	18 03 02	L	18	1.7	9.4
				C	5.8	0.71	12
	S(A)	04 28 46.4	17 57 15	L	2.0	0.61	31
				C	1.1	0.21	19
	S(B)	04 28 46.7	17 56 53	L	1.2	0.34	28
				C	0.47	0.29	61

[a] The four L band frequencies are represented by an average value.

[b] Percentage polarization.

[c] Sources 1–4 were not visible in polarization maps at C band.

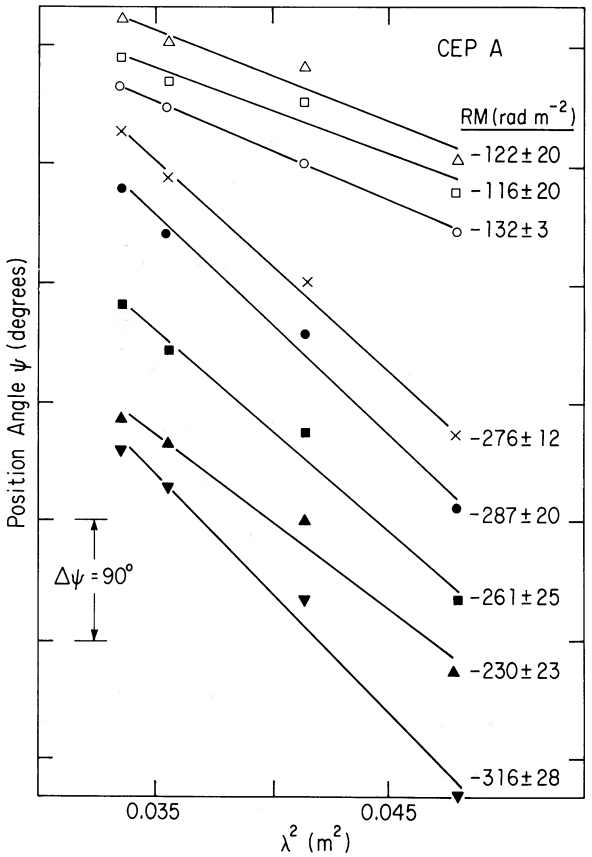

FIG. 1.—Position angle of linear polarization vs. squared wavelength for the extragalactic sources in the Cep A field. Only L band values are shown and rotation measures from least-squares fits are displayed. Error bars are smaller than the plotted points. Symbols used for the plotted data points correspond to source symbols in Fig. 2 and to source numbers in Table 3 as follows: 1 = ○; 2 = ●; 3 = △; 4 = □; 5a = ▼; 5b = ▲; 6 = ×; 7 = ■.

Therefore, it is unclear at present what boundaries may finally be set for the flows in either L1551 or Cep A.

Since rotation measures in this area of the sky are generally large and negative, and this line of sight is in the galactic plane ($l^{II} \approx 110°$, $b^{II} \approx 2°$), the cloud is probably not responsible for the approximate magnitude and sign of the RMs we obtained. More likely, the cloud determines the difference in RM between the two groupings of values. This difference of ~ 150 rad m^{-2} on a $\sim 10'$ angular scale is much larger than differences $\lesssim 15$ rad m^{-2} on the same angular scale over arbitrarily chosen lines of sight (Simonetti, Cordes, and Spangler 1984; Simonetti and Cordes 1986). However, deducing a magnetic field value by comparing lines of sight would be mainly guesswork, without more definite information on localizable differences in the lines of sight. The molecular flow may be responsible. In this regard, aspects of the following discussion on L1551 may apply here as well. At present, however, the large differences in rotation measures through Cep A are unexplained but seem to be due to material with at least the same angular scale as the molecular cloud.

b) L1551

High resolution was critical in studying individual components in the L1551 sources since the resulting rotation measures are small and we sought greater precision than for the Cep A sources. Given the relatively large degree of polarization in the two polarized components of the S source, and the agreement in their respective RMs, we believe intrinsic effects are negligible for the S source. For the N source we argue that the nearly equal polarization percentages in the L and C bands also signify small internal Faraday rotation. Therefore, we attribute the difference in measured RM values for the L1551 sources entirely to galactic effects.

We assume in the following discussion that the difference in rotation measure of the N and S sources ($\Delta RM = 30 \pm 7$ rad m^{-2}) is probably determined by the high-velocity flow in L1551. First of all, the rotation measure difference between two randomly selected lines of sight separated by 7′ is typically much less in magnitude than 30 rad m^{-2}. The fairly large galactic latitude ($l^{II} \approx 179°$, $b^{II} \approx -20°$), the small RMs in general for this area, our small RM values, and observations suggesting this direction is empty of obscuring material other than L1551 (Straižys and Meištas 1980), imply that the most important influence on ΔRM may lie within the L1551 region. Both extragalactic sources are seen through the dark CO cloud (Snell 1979), and therefore both lines of sight pierce the outer, theoretically ionized skin of the cloud. The only identifiable difference between both radiation pathways is the high-velocity molecular flow seen in front of the N source. Henceforth, we will assume ΔRM is attributable to the presence of the high-velocity flow, and we will discuss what may be learned about the magnetic field strength in the flow region.

The high-velocity CO flow mapped by Snell, Loren, and Plambeck (1980), extends over ~ 1.0 pc. The red and blue-

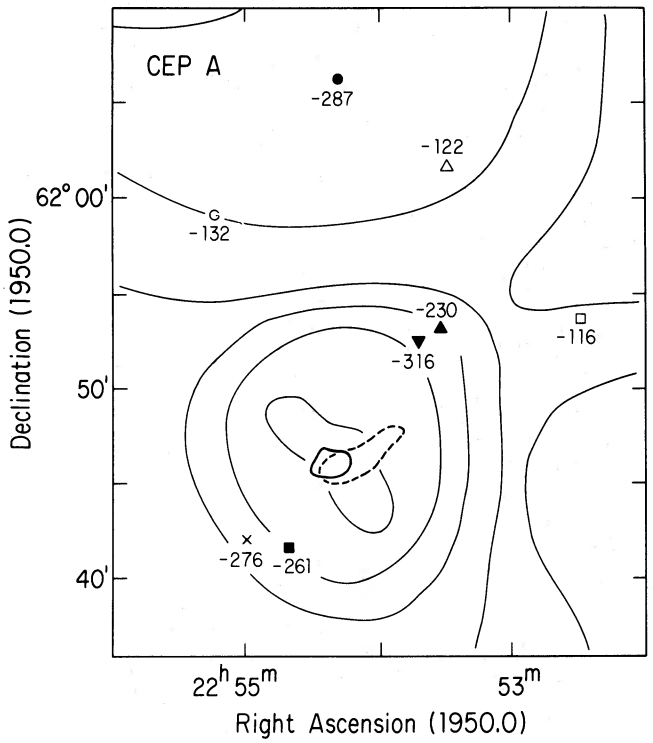

FIG. 2.—Map of the Cep A field. Positions of background extragalactic sources are labeled by their rotation measures (rad m^{-2}). The high-velocity CO lobes of Rodríguez, Ho, and Moran (1980) are represented by a dark outline and dashed outline for the blue and redshifted lobes, respectively. Light lines are temperature contours of CO emission from Sargent (1977; contour levels in decreasing order: 15, 10, 7.5, 5, 2.5 K).

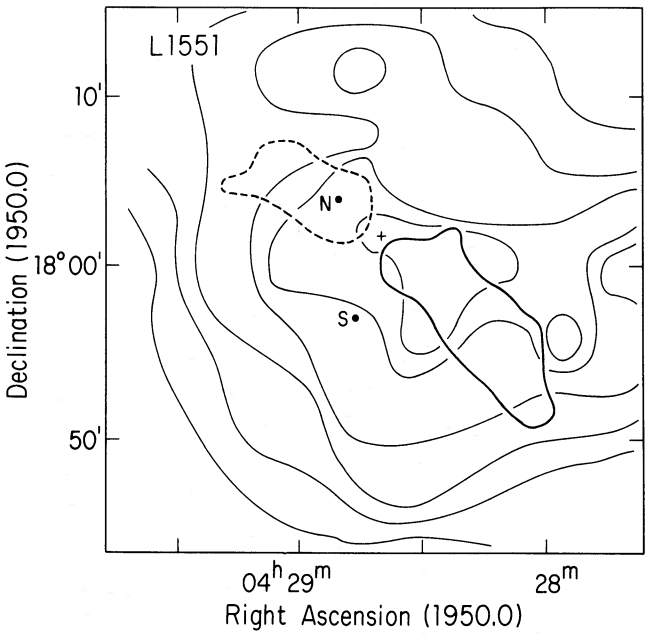

FIG. 3.—Map of L1551 field. The positions of the north and south background sources are labeled by N and S. The high-velocity CO lobes (Snell, Loren, and Plambeck 1980) are displayed as in Fig. 2. IRS 5, the apparent source of the outflow, is represented by a cross. The light lines are CO temperature contours (levels; 2–12 K, with increments of 2 K) from Snell (1979).

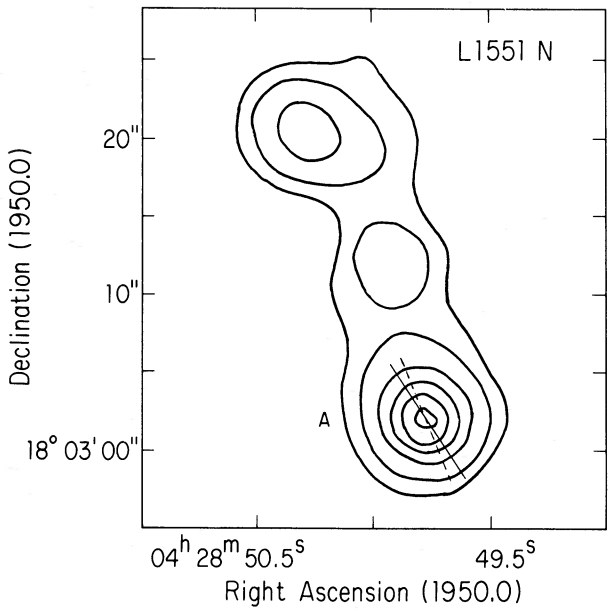

FIG. 4.—Total intensity map at 1640 MHz of the N source in L1551 where "A" is the polarized component. Contours are at 3%, 10%, 30%, 50%, 70%, and 90% of the peak intensity of 15.9 mJy per beam. Polarization vectors (of arbitrary length) are shown at the peak of intensity for 1640 MHz (*solid line*) and 1370 MHz (*dashed line*).

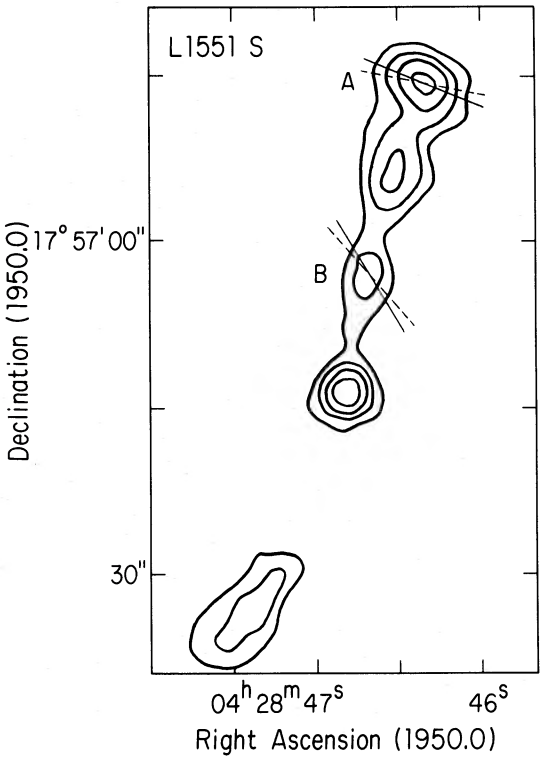

FIG. 5

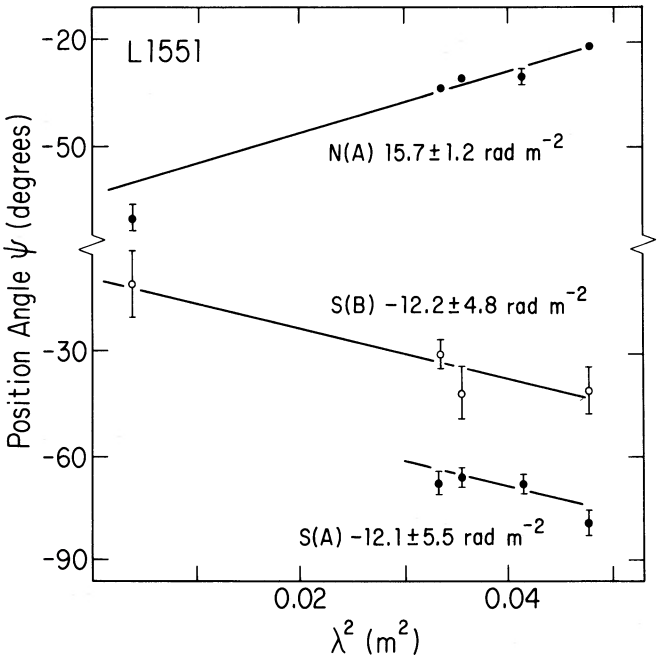

FIG. 6

FIG. 5.—Total intensity map at 1640 MHz of the S source in L1551. The polarized components are labeled "A" and "B." Contours levels are 3%, 5%, 7%, and 9% of 15.9 mJy per beam. Polarization vectors (of arbitrary length) are shown at the peak of intensity for 1640 MHz (*solid line*) and 1370 MHz (*dashed line*).

FIG. 6.—Position angle of linear polarization vs. squared wavelength for the sources in the L1551 field. These values are from the pixel of peak polarized intensity in the labeled component. The rotation measure is displayed.

shifted lobes (Fig. 3) are ~ 0.1 pc in width, have relative radial velocities of ~ 15 km s^{-1}, and involve 0.3 $M_\odot$ of material. Herbig-Haro objects (HH 28, HH 29) seen in the blueshifted lobe have detectable proper motions which projected backward cross at an origin near IRS 5, the apparent source of the outflow (Cudworth and Herbig 1979). At a distance of 160 pc, the observed HH proper motions correspond to transverse velocities in excess of ~ 150 km s^{-1}. These transverse velocities, combined with observed radial velocities of about -50 km s^{-1} (Strom, Grasdalen, and Strom 1974), imply the flow is seen at an angle of $\sim 75°$ to the line of sight.

Using only the above information, it is possible to make a few useful statements and put some limits, albeit rather weak ones, on the magnetic field strength in the cloud. That the observed ΔRM ≈ 30 rad m^{-2} is due to the presence of more Faraday-active material (i.e., larger $|\langle n_e B_\parallel \rangle|$) in the high-velocity flow region, rather than in the ambient cloud, is clear from the following argument. Snell (1979) estimates the density of the L1551 cloud at $n_{H_2} \approx 10^4$–10^5 cm^{-3} in the core, dropping to $\sim 10^2$ cm^{-3} at a radius of ~ 1 pc. Assuming a fractional ionization $x_e \approx 10^{-7}$, typical of molecular cloud interiors, and a 1 mG magnetic field strength, equation (1) implies a rotation measure through 0.1 pc of ambient cloud material,

$$\delta \mathrm{RM}_{\mathrm{amb}} = 0.081 \left(\frac{n_{H_2}}{10^4 \text{ cm}^{-3}}\right)\left(\frac{x_e}{10^{-7}}\right)\left(\frac{B_\parallel}{1 \text{ mG}}\right) \times \left(\frac{l}{0.1 \text{ pc}}\right) \text{rad m}^{-2}\,, \quad (3)$$

which is much less than the observed ΔRM for any reasonable choice of parameters. Therefore, the observed ΔRM for the two lines of sight must be dominated by Faraday rotation within the molecular flow region. Furthermore, unless $B_\parallel$(lobe) is very large ($\gtrsim 1$ G) the ionization and hence the electron density within the flow lobe n_e(lobe) must be much larger than in the ambient cloud. Requiring the magnetic pressure within the cloud to be comparable to or less than the gas pressure implies $|B_\parallel| \lesssim 0.1$ mG, but this applies to the ambient cloud medium; it is possible the field could be larger in the lobe, and even drive the expanding flow, but a 1 G field strength is probably much too large.

Figure 7 illustrates, for the flow region, the minimum $B_\parallel$ consistent with the observations. Below $n_e \approx 10$–100 cm^{-3}, the minimum $B_\parallel$ is

$$(B_\parallel)_{\min} = 270 \left(\frac{n_e}{\text{cm}^{-3}}\right)^{-1} \mu\text{G}\,, \quad (4)$$

determined by the maximum path length through the lobe, $l \lesssim 0.1$ pc. At larger n_e, the absence of radio bremsstrahlung emission in our maps at the 3 σ level sets an upper limit to the emission measure at

$$\int n_e^2\, dl < 3400 \left(\frac{T_e}{10^4 \text{ K}}\right)^{0.35} f_B^{-1} \text{ cm}^{-6} \text{ pc}\,, \quad (5)$$

where f_B is the beam filling factor of the emission. Equivalently, assuming $f_B = 1$, the implied electron column density and our observed ΔRM yield

$$(B_\parallel)_{\min} = 1.1 \left(\frac{T_e}{10^4 \text{ K}}\right)^{-0.35} \left(\frac{n_e}{10^2 \text{ cm}^{-3}}\right) \mu\text{G} \quad (6)$$

for the minimum $B_\parallel$ at large electron density. The assumption $f_B = 1$ is good for our purposes: unless regions of such high n_e essentially cover the projected lobe area, it is unlikely our line of sight to the N source passes through such a region. We emphasize that the magnetic field values given by equations (4) and (6) are minimum values arrived at by adopting the largest possible contribution to ΔRM from the electron column density.

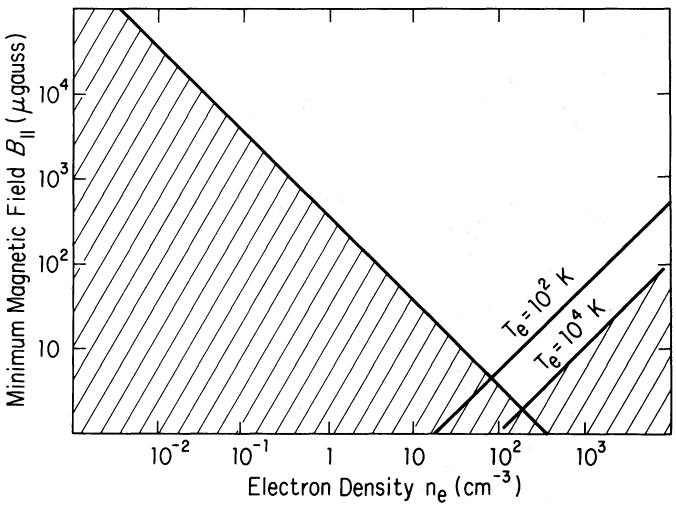

FIG. 7.—The minimum allowable $B_\parallel$ within the flow region of L1551 vs. the spatially coincident electron density, given a rotation measure through the lobe of 30 rad m^{-2}. Cross-hatched areas are excluded for a uniformly filled path length of 0.1 pc at low n_e and by the absence of free-free continuum emission at large n_e (temperature-dependent).

We now turn to a discussion of theoretical models for high-velocity flows and other observations of L1551 in an attempt to delineate further limits on n_e and, therefore, $B_\parallel$. Shock ionization seems the most likely candidate for a source of free electrons in the flow lobes. We comment upon the possibility of shock ionization in four models.

Draine (1980) has proposed a model where the observed high-velocity lobes are part of a magnetic-pressure–driven, expanding bubble. The shell of swept-up material moves at a speed, for L1551, of $V \approx 15$ km s^{-1}, or perhaps as large as 58 km s^{-1} if the flow is at 75° to the line of sight. A shock is set up at the exterior surface of the bubble, but no substantial ionization will take place at such shock speeds in molecular gas; i.e., where $v_s < 50$ km s^{-1} (McKee, Chernoff, and Hollenbach 1984, esp. p. 111). We note there is apparently a fairly sharp velocity boundary beyond which substantial shock ionization does take place. It is not clear exactly what velocity to attribute to the bubble expansion at the position of the N source, but it must be less than at the head of the lobes if a bipolar flow is the result, as observed. The shock velocity relevant to our line of sight through the lobe for an expanding bubble model is probably less than 50 km s^{-1}. At these shock velocities, changes in ionization by factors of ~ 5–10 over ambient can take place. From Figure 7, such low n_e values correspond to a minimum $B_\parallel \approx 10$–100 mG if the path length is the maximum of 0.1 pc. Therefore, $B_\parallel$ within the thinner shock region must be larger than 10–100 mG. Such a field within the swept-up shell would greatly complicate the model unless the field within the expanding cavity is of approximately the same strength; i.e., the driving magnetic pressure in the model comes from a greater than 10–100 mG field. However, such a large field value yields results inconsistent with the observed flow. The force on

the shell, given by Draine's equation (6), is

$$\frac{d}{dt}(MV) = 4\pi R^2 \frac{(B^2 - B_0^2)}{24\pi} \approx \rho_0 \frac{4}{3} \pi R^3 V \left(\frac{V}{R}\right),$$

where M, V, and R are the shell mass, velocity, and radius; B is the field within the expanding cavity; B_0 is the ambient cloud field. We have estimated the above rate of change of momentum assuming a constant V, but increasing M over the dynamical lifetime of the flow, where $\rho_0 \approx m_{H_2} \times 10^4$ cm^{-3} is the ambient cloud mass density. Assuming $B_0 \approx 1$ mG and $B \gtrsim$ 10–100 mG, we find $V \gtrsim$ 100–1000 km s^{-1}, much larger than the observed $V \approx$ 15–50 km s^{-1}. Using the observationally determined $M \approx 0.3\ M_\odot$ (Snell, Loren, and Plambeck 1980), instead of the above estimate based on an ambient density and shell radius, yields an even greater V.

In a stellar-wind driven expansion (e.g., Snell, Loren, and Plambeck 1980; Königl 1982) the above comments concerning ionization exterior to the expanding cavity also apply. However, within the bubble, a wind of velocity approaching $\sim$200 km s^{-1} is hypothesized to explain the speed of the HH objects (a problem unaddressed by Draine's model). This wind may fill an evacuated cavity or it may encounter and push against many small knots of material. For now, we ignore the existence of knots and assume the cavity has been swept clean of ambient cloud material. Then there must be a shock with $v_s >$ 50 km s^{-1} at the interior wall of the swept-up shell where ionization is substantial. At $v_s >$ 100 km s^{-1} the postshock electron column density (line of sight normal to the shock surface) is $\sim 10^{18}$ cm^{-2}, relatively independent of the detailed state of the preshock gas (McKee, Chernoff, and Hollenbach 1984; Shull and McKee 1979). With the observed ΔRM, this electron column density implies, using equation (1),

$$B_\parallel \approx \left(\frac{0.1}{N_s \langle \sec \theta_s \rangle}\right) \text{mG}, \qquad (7)$$

where $N_s\langle \sec \theta_s \rangle$ is the number of shocks adjusted by an average geometrical factor (θ_s is the angle of a shock's normal to the line of sight) and is limited to $N_s\langle \sec \theta_s \rangle \lesssim 100$ by the absence of radio continuum in our maps ($T_e = 10^4$ K, $n_e = 10^2$ cm^{-3}). The simplest evacuated-cavity model has $N_s = 2$.

In the model discussed by Pudritz and Norman (e.g., Pudritz and Norman 1986) the molecular flow originates from the surface of a rotating molecular accretion disk and reaches a terminal velocity $\lesssim$50 km s^{-1} before encountering denser ambient material. Furthermore, an ionized wind of terminal velocity $\gtrsim$200 km s^{-1} leaves the disk surface closer to the central protostar. As in the above discussion of Draine's model, the slower molecular gas has little potential for causing substantial shock ionization. However, the higher velocity wind, upon encountering the slower moving molecular flow, or ambient material, will produce substantial shock ionization, and equation (7) is relevant.

In connection with these last two models we mention one potential, but probably negligible, source of Faraday rotation independent of any shocks: the ionized, driving stellar wind in Königl's model, or the central, ionized wind in the model of Pudritz and Norman. For discussion, we use recent radio and optical observations of L1551 to estimate the electron density, n_e(lobe wind), of these winds at the interior of the extended bipolar lobes. An estimate of B(lobe wind) is more model dependent.

From radio continuum observations of L1551, Snell *et al.* (1985) describe a jet, centered on IRS 5, of length 20″ and width less than 5″, which, combined with a flux density, implies an electron density n_e(jet) $\approx 2 \times 10^3$ cm^{-3} (for a width of 5″). In the southwest direction, scattered light from what appears to be the "walls" of an interior cavity and emission from shock-ionized gas interior to those walls both suggest the jet expands beyond 10″ from IRS 5 and a cavity of constant width $\sim$180″ appears between 2′ and 10′ from IRS 5. Such an expansion is consistent with the stellar-wind driven models. In the model of Pudritz and Norman the ionized wind originates from the central $\sim$1% of the molecular disk, after which the expansion of both the ionized wind and outer molecular flow are guided by the magnetic field geometry, taken to be hourglass in shape and centered on the disk. Thus, in this model the ionized wind may fill only a small core of the extended lobes. In any case, we feel the observational evidence favors a high-velocity wind, originally a jet very near IRS 5, expanding and filling most of the interior of the extended lobe to the southwest, and presumably to the northeast, of IRS 5. Assuming the jet velocity does not change during the expansion these observations imply n_e(lobe wind) $\approx (5/180)^2 n_e$(jet) ≈ 1 cm^{-3}, if *no* recombination occurs during the outflow.

From Figure 7, for an electron density of n_e(lobe wind) ≈ 1 cm^{-3} we require a minimum $B_\parallel$(lobe wind) of $\sim 350\ \mu$G if the wind alone is to account for the observed RM. Assuming magnetic flux conservation during the expansion of the outflow, we have B(jet) $\gtrsim (180/5)^2 B$(lobe wind) or B(jet) $\gtrsim$ 450 mG. First, assume the jet is a stellar wind collimated by a disk of inner radius $\lesssim$100 AU, consistent with the observed thickness of the radio jet and obscuration of the optical jet at less than 1″ to the northeast of IRS 5 (Snell *et al.* 1985). As discussed by Michel and Yahil (1973), the magnetic field carried to large distances by a stellar wind falls in magnitude as r^{-1}. This implies $B(\text{star}) \approx B(R_\odot) \approx (100\ \text{AU}/R_\odot)$ 450 mG or $B(\text{star}) \approx 10^4$ G, which seems excessive, although kilogauss fields may be reached in some transient period during star formation, perhaps coincident with the bipolar nebula stage. On the other hand, if we assume the ionized wind comes from a magnetized molecular disk formed from compressed ambient material, then the expected magnetic field in the disk will be only somewhat larger than the ambient value; i.e., B(disk) $\approx$ 10 mG (Pudritz 1985). In this scenario it is hard to expect the field to reach the B(jet) $\gtrsim$ 450 mG required above. In conclusion, it seems likely that any contribution to the observed rotation measure from an ionized wind is small.

The fourth model invokes many dense knots moving outward from a central source (e.g., Chevalier 1980; Norman and Silk 1979) to explain the observed high-velocity molecular gas, rather than the pressure-driven shell or uniform flow of material of the first three models. The knots are clumps of ambient material accelerated close to the star, perhaps by a wind or an unknown mechanism. These "bullets" travel $\sim$1 pc in a typical cloud (Norman and Silk 1979) and some may be the visible HH objects. By avoiding a bubble scenario, this model may accommodate the difference in the extent of high-velocity OH and CO in L1551, whereas expanding shells may not.

The highest velocity knots ($v \approx 100$ km s^{-1}) will have bow shocks with properties as discussed above for the high-velocity shock at the interior wall of a bubble. But the majority of knots must be moving at $v <$ 50 km s^{-1} to account for the mass of molecular material seen at those velocities. Ionization around

these knots will be small. Therefore, for this model, the electron column density through the flow region is determined by the number of knots along the line of sight with $v > 50$ km s^{-1}. If we once again define N_s to be the number of shocks along the path length produced by such high-velocity knots and take into account the obliquity of each shock to the line of sight, then equation (7) yields the magnetic field within these shock regions.

V. SUMMARY

Having obtained significant differences in Faraday rotation measure between various lines of sight through Cep A and L1551, we looked for explanations in terms of electron density and magnetic field variations within the clouds.

The Cep A case is difficult to interpret without further knowledge of the environment within Cep A, so the large RM variations are at present unexplainable.

The L1551 situation is very interesting, given the fact that one line of sight passes through the NE lobe of the high-velocity molecular flow within the cloud. Based upon a discussion of various models for the molecular flow, it seems likely that the magnetic field strength in the flow region may be as great as ~ 0.1 mG. It is apparent that much greater than ambient electron densities are required if extremely large magnetic field values, and subsequent conclusions inconsistent with observations are to be avoided. Substantial shock ionization must take place requiring relative velocities in excess of 50 km s^{-1}.

At this time, very little is known observationally about the ionization state in these high-velocity molecular flow regions. Free-electron column densities are probably small, but perhaps radio recombination line observations could be useful in detecting or better constraining the column density. Another potential line of investigation might be a search for H I Zeeman splitting as a way to get a direct handle on the field strength.

Currently, we plan to search for more extragalactic sources outside the boundaries of L1551 for a comparison with those we have observed and to investigate other candidate molecular flows where extragalactic sources may be found. Where a number of extragalactic sources lie behind a bipolar flow, it may be possible to test the model of Pudritz and Norman for the production of the gas outflow. Because of the azimuthal field produced by the rotation of the molecular disk, rotation measures of opposite sign should be seen for adjacent quadrants defined by the rotation axis and plane.

The authors wish to thank the staff of the National Radio Astronomy Observatory for their support. The authors also wish to acknowledge useful discussions with S. Beckwith and D. Chernoff. This research was supported by the National Astronomy and Ionosphere Center, which is operated by Cornell University under contract with the National Science Foundation.

REFERENCES

Bridle, A. H. 1982, in *Synthesis Mapping, Proc. NRAO-VLA Workshop*, ed. A. R. Thompson and L. R. D'Addario (NRAO), p. 14–1.
Chernoff, D. F., Hollenbach, D. J., and McKee, C. F. 1982, *Ap. J. (Letters)*, **259**, L97.
Chevalier, R. A. 1980, *Ap. Letters*, **21**, 57.
Condon, J. J., and Mitchell, K. J. 1982, *A.J.*, **87**, 1429.
Cudworth, K. M., and Herbig, G. 1979, *A.J.*, **84**, 548.
Draine, B. T. 1983, *Ap. J.*, **270**, 519.
Draine, B. T., and Roberge, W. G. 1982, *Ap. J. (Letters)*, **259**, L91.
Hughes, V. A., and Wouterloot, J. G. A. 1984, *Ap. J.*, **276**, 204.
Königl, A. 1982, *Ap. J.*, **261**, 115.
McKee, C. F., Chernoff, D. F., and Hollenbach, D. J. 1984, in *Galactic and Extragalactic Infrared Spectroscopy*, ed. M. F. Kessler and J. P. Phillips (Dordrecht: Reidel), p. 103.
Michel, F. C., and Yahil, A. 1973, *Ap. J.*, **179**, 771.
Mirabel, I. F., Rodríguez, L. F., Cantó, J., and Arnal, M. 1984, *Bull. AAS*, **16**, 522.
Mouschovias, T. Ch. 1976, *Ap. J.*, **207**, 141.
Norman, C., and Silk, J. 1979, *Ap. J.*, **228**, 197.
Pudritz, R. E. 1985, *Ap. J.*, **293**, 216.
Pudritz, R. E., and Norman, C. A. 1983, *Ap. J.*, **274**, 677.
———. 1986, *Ap. J.*, **301**, 571.
Rodríguez, L. F., Ho, P. T. P., and Moran, J. M. 1980, *Ap. J. (Letters)*, **240**, L149.
Sargent, A. I. 1977, *Ap. J.*, **218**, 736.
Shull, J. M., and McKee, C. F. 1979, *Ap. J.*, **227**, 131.
Simard-Normandin, M., Kronberg, P. P., and Button, S. 1981, *Ap. J. Suppl.*, **45**, 97.
Simonetti, J. H., and Cordes, J. M. 1986, in preparation.
Simonetti, J. H., Cordes, J. M., and Spangler, S. R. 1984, *Ap. J.*, **284**, 126.
Snell, R. L. 1979, Ph.D. thesis, University of Texas.
Snell, R. L., Bally, J., Strom, S. E., and Strom, K. M. 1985, *Ap. J.*, **290**, 587.
Snell, R. L., Loren, R. B., and Plambeck, R. L. 1980, *Ap. J. (Letters)*, **239**, L17.
Straižys, V., and Meištas, E. 1980, *Acta. Astr.*, **30**, 541.
Strom, S. E., Grasdalen, G. L., and Strom, K. M. 1974, *Ap. J.*, **191**, 111.
Vrba, F. J., Strom, S. E., and Strom, K. M. 1976, *A.J.*, **81**, 958.
Wardle, J. F. C., and Kronberg, P. P. 1974, *Ap. J.*, **194**, 249.
Wouterloot, J. G. A., Habing, H. J., and Herman, J. 1980, *Astr. Ap.*, **81**, L11.

JAMES M. CORDES: Space Sciences Building, Cornell University, Ithaca, NY 14853

JOHN H. SIMONETTI: National Radio Astronomy Observatory, Edgemont Road, Charlottesville, VA 22903